Mechanics of Advanced Materials and Structures, 13:249–266, 2006

ISSN: 1537-6494 print / 1537-6532 online
DOI: 10.1080/15376490600582750

Taylor & Francis
Taylor & Francis Group

Discrete Layer Solution to Free Vibrations of Functionally Graded Magneto-Electro-Elastic Plates

Fernando Ramirez and Paul R. Heyliger
Department of Civil Engineering, Colorado State University, Fort Collins, Colorado, USA

Ernian Pan
Department of Civil Engineering, University of Akron, Akron, Ohio, USA

Natural frequencies of orthotropic magneto-electro-elastic graded composite plates are determined using a discrete layer model with two different approaches. In the first, the functions describing the gradation of the materials properties through the thickness of the plate are incorporated into the governing equations. In the second approach, the plate is divided into a finite number of homogeneous layers. The model is validated by comparing the natural frequencies of a simply supported Al/ZrO_2 graded square plate with the exact solution. Excellent agreement is obtained. Rectangular plates with different boundary conditions, aspect ratios, and made of different types of composite materials are also considered: Al/ZrO_2 and $BaTiO_3/CoFe_2O_4$ plates for which the volume fraction of the phases change as a function of the z coordinate, graphite/epoxy plates with the orientation of the fibers changing through the thickness of the plate, and plates having an exponential variation of the material properties. Applicability of the proposed model is not limited to specific boundary conditions and gradation functions.

1. INTRODUCTION

Composite materials consisting of piezoelectric and magneto-strictive phases exhibit a magneto-electric effect which is not present in the individual constituents [1]. These composites show significant interactions between the elastic, electric, and magnetic fields due to the coupled nature of the constitutive equations. These laminates have direct application in sensing and actuating devices, such as damping and control of vibrations in structures. Several methods for determining the effective moduli of magneto-electro-elastic composite media have been published by Benveniste [1], Huang and Kuo [2], Li and Dunn [3], Aboudi [4], and Tan and Tong [5]. Research on the behavior of laminated plates composed by elastic, piezoelectric, and/or magnetostrictive layers is relatively recent. The exact closed-form solution for three-dimensional simply supported magneto-electro-elastic laminates was presented by Pan [6] based on the quasi-Stroh formalism and the propagator matrix method. Later, Pan and Heyliger [7, 8] extended that solution to the corresponding free vibration problem, and to the static cylindrical bending of magneto-electro-elastic laminates. An approximate solution based on a discrete layer model was also obtained by Heyliger and Pan [9] and Heyliger et al. [10] for the cases of two and three-dimensional magneto-electro-elastic laminates. More recently, Jiang and Ding [11] presented an analytical solution for the study of beams, Lage et al. [12] developed a layerwise mixed finite element model for plates, and Latheswary et al. [13] studied the dynamic response of moderately thick composite plates.

Functionally graded materials (FGM) are characterized by a gradual change in properties within the specimen as a function of the position coordinates. These materials have been presented as an alternative to laminated composite materials that show a mismatch in properties at material interfaces. This material discontinuity in laminated composite materials leads to large interlaminar stresses and the possibility of initiation and propagation of cracks [14]. This problem is reduced in FGM because of the gradual change in mechanical properties as a function of position through the composite laminate.

Studies of the static and dynamic behavior of composite plates made of FGM have seen a small but useful number of investigations. Reddy [14] presented Navier's solutions of rectangular plates and finite element models based on the third-order shear deformation plate theory for the analysis of through-thickness functionally graded plates, with the modulus of elasticity of the plate varying according to a power-law distribution in terms of the volume fractions of the constituents. Cheng and Batra [15] studied the deflection of functionally graded plates using the first and higher-order shear deformation theories, and its relationship to that of an equivalent homogeneous Kirchhoff plate. Cheng and Batra [16] also used Reddy's third-order plate theory to study buckling and steady state vibrations of a simply supported functionally gradient isotropic polygonal plate resting

Received 18 May 2005; accepted 19 December 2005.
Address correspondence to Fernando Ramirez, Department of Civil Engineering, Colorado State University, Fort Collins, CO, 80523. E-mail: framirez@engr.colostate.edu

on a Winkler-Pasternak elastic foundation and subjected to uniform in-plane hydrostatic loads. They later obtained a closed form solution for the thermomechanical deformations of an isotropic linear thermoelastic functionally graded elliptic plate [17]. Vel and Batra [18, 19] obtained exact solutions for three-dimensional deformations of a simply supported functionally graded rectangular plate subjected to mechanical and thermal loads, and for free and forced vibrations of simply supported functionally graded rectangular plates. In both of these studies, two-constituent metalceramic functionally graded rectangular plates were considered with a power law through-the-thickness variation of the volume fractions of the constituents, with the effective material properties at a point estimated by either the Mori-Tanaka or self-consistent schemes. Ferreira et al. [20] used the meshless collocation method, the multiquadric radial basis functions and a third-order shear deformation theory to analyze static deformations of functionally graded square plates of different aspect ratios. Batra and Jin [21] studied the free vibrations of functionally graded anisotropic graphite/epoxy plates, with the orientation of the fibers varying through the thickness of the plate. The solution presented was based on the first order shear deformation theory coupled with the finite element method. Qian et al. [22] analyzed the static deformations, and free and forced vibrations of thick simply supported rectangular graded elastic Al/ZrO_2 plates by using a higher-order shear and normal deformable plate theory and a meshless local Petrov-Galerkin method. They compared the results to available exact solutions obtaining excellent agreement. Pan [23] presented an exact solution for three-dimensional, anisotropic, linearly elastic, and functionally graded rectangular composite laminates under simply supported edge conditions. The solution was expressed in terms of the pseudo-Stroh formalism, and the composite laminate made of multilayered functionally graded materials with their properties varying exponentially in the thickness direction. Ramirez et al. [24] derived a discrete layer solution for the static analysis of FGM plates with different boundary conditions, and applicable to materials having any type of gradation function describing the through-thickness variation of the material properties.

Studies of vibration analysis involving magneto-electro-elastic composite media are limited. Yang et al. [25] investigated the non-linear bending behavior of functionally graded plates that are bonded with piezoelectric actuator layers and subjected to transverse loads and a temperature gradient based on Reddy's higher-order shear deformation plate theory. They assumed material properties to be graded in the thickness direction according to a power-law distribution in terms of the volume fractions of the constituents. Woo and Meguid [26] presented an analytical solution for the coupled large deflection of plates and shallow shells made of functionally graded materials under transverse mechanical loads and a temperature field, results indicated that thermomechanical coupling effects play a major role in dictating the response of functionally graded shells. Liew et al. [27] derived finite element formulations for static and dynamic analysis and the control of functionally graded material (FGM) plates under environments subjected to a temperature gradient, using linear piezoelectricity theory and first-order shear deformation theory. Buchanan [28] published a comparison of the natural frequencies between layered and different multiphase models for magneto-electro-elastic $BaTiO_3/CoFe_2O_4$ plates, the frequencies were determined using finite element analysis. Chen et al. [29] derived two independent state equations to determine the natural frequencies of piezoelectric functionally graded rectangular plates, with all the properties varying through the thickness of the laminate according to a law of mixtures. The free vibration problem of simply supported plates was solved by dividing the plate into thin layers having constant properties. Chen et al. [30] extended this work to the solution of the free vibration problem of simply supported non-homogeneous magneto-electro-elastic plates. Once again a law of mixtures was employed for the functionally graded model of all the properties, except for the magnetoelectric coefficients that were obtained by fitting a curve to the results presented by Li and Dunn [3].

In this paper, a general discrete layer model is developed for the free vibration analysis of elastic, piezoelectric, magnetostrictive, and magneto-electro-elastic composite graded plates. The gradation functions describing the through-thickness variation of material properties are incorporated into the governing equations of equilibrium for each discrete layer, which are then solved by using continuous functions to approximate the three displacement components, the electric potential, and the magnetic potential within each layer. The present approach is validated by calculating the natural frequencies of simply supported square Al/ZrO_2 graded plates with known exact solutions [18, 22]. Natural frequencies of composites graded plates having different boundary conditions, aspect ratios, and gradation types are obtained using the proposed model. The numerical examples presented here are solved using two different approaches. First, the gradation functions are incorporated into the governing equations and analytically or numerically integrated before assembling the stiffness and mass matrices and before solving the eigenvalue problem. In the second approach, the plates are discretized into a finite number of homogenous layers. The types of gradation models considered here are: 1) Al/ZrO_2 graded plates with the volume fraction of the constituents varying as functions of the thickness coordinate, and with effective material properties at any height z within the plate determined by using the Mori-Tanaka scheme [19, 22], 2) rectangular plates exhibiting an exponential variation of the elastic stiffness components as a function of the out-of-plane coordinate [23], 3) graphite/epoxy fiber-reinforced plates in which the fiber orientation varies across the laminate thickness, and with effective moduli determined by tensor transformations [21], and 4) $BaTiO_3/CoFe_2O_4$ fibrous composite plates, consisting of a magnetostrictive matrix with a dispersed fibrous piezoelectric phase, with the volume fraction of the constituents varying through the thickness of the plate, and with effective material properties obtained using the

Mori-Tanaka mean field approach coupled with the magneto-electroelastic Eshelby tensor [3].

2. THEORY

2.1. Problem Description

Free vibration behavior of elastic, piezoelectric, magnetostrictive, and magneto-electro-elastic plates having specific variations of material properties through the thickness is studied to determine their natural frequencies. The geometry of the rectangular plates is described by attaching a Cartesian coordinate system to the lower left corner of the laminate. The length of the plate L_x is in the direction of the x coordinate axis, while the directions of the width L_y and total thickness H are coincident with the directions of the y and z coordinate axes respectively. Analyses are performed by discretizing the plates into a finite number of layers N, each layer with individual thickness h_i, h_1 being the bottom layer, and h_N the top layer.

Behavior of plates having different through-thickness variation of the material properties are considered: 1) composites made of two isotropic elastic materials in which the volume fraction of the constituents varies through the thickness of the plate, 2) elastic orthotropic plates exhibiting exponential variation of material properties as a function of the z coordinate, 3) elastic fiber-reinforced plates in which the orientation of the fibers continuously changes through the thickness of the plate, and 4) magneto-electro-elastic composite plates formed by combining piezoelectric and magnetostrictive materials having a smooth variation of the constituent volume fractions with the thickness coordinate of the laminate.

2.2 Governing Equations

Considering the coupled behavior among elastic, electric, and magnetic fields exhibited by magneto-electro-elastic laminates, and including the through-thickness variation of the material properties, the constitutive equations for the anisotropic and linearly elastic layers in the laminate are given by [31]:

$$\sigma_i = C_{ik}(z)S_k - e_{ki}(z)E_k - q_{ki}(z)H_k \tag{1}$$

$$D_i = e_{ik}(z)S_k + \epsilon_{ik}(z)E_k + d_{ik}(z)H_k \tag{2}$$

$$B_i = q_{ik}(z)S_k + d_{ik}(z)E_k + \mu_{ik}(z)H_k \tag{3}$$

where σ_i, D_i, and B_i denote the components of stress, electric displacement, and magnetic flux. The symbols $C_{ij}(z)$, $\epsilon_{ij}(z)$, and $\mu_{ij}(z)$ are the components of elastic stiffness, and the dielectric and magnetic permittivity as functions of the z coordinate; γ_k, E_k, and H_k denote the components of linear strain, electric field, and magnetic field; and $e_{ij}(z)$, $q_{ij}(z)$, and $d_{ij}(z)$ are the piezoelectric, piezomagnetic, and magnetoelectric coefficients which vary through the thickness of the plate. The standard engineering contraction indices has been used here for the elastic variables (i.e. $\gamma_4 = \gamma_{23}$, etc.). The components of the rotated material property tensors for an orthotropic material are given in matrix form as

$$\left[\begin{array}{cccccc|ccc|ccc}
C_{11}(z) & C_{12}(z) & C_{13}(z) & 0 & 0 & C_{16}(z) & 0 & 0 & e_{31}(z) & 0 & 0 & q_{31}(z) \\
C_{12}(z) & C_{22}(z) & C_{23}(z) & 0 & 0 & C_{26}(z) & 0 & 0 & e_{32}(z) & 0 & 0 & q_{32}(z) \\
C_{13}(z) & C_{23}(z) & C_{33}(z) & 0 & 0 & C_{36}(z) & 0 & 0 & e_{33}(z) & 0 & 0 & q_{33}(z) \\
0 & 0 & 0 & C_{44}(z) & C_{45}(z) & 0 & e_{14}(z) & e_{24}(z) & 0 & q_{14}(z) & q_{24}(z) & 0 \\
0 & 0 & 0 & C_{45}(z) & C_{55}(z) & 0 & e_{15}(z) & e_{25}(z) & 0 & q_{15}(z) & q_{25}(z) & 0 \\
C_{16}(z) & C_{26}(z) & C_{36}(z) & 0 & 0 & C_{66}(z) & 0 & 0 & 0 & 0 & 0 & 0 \\
\hline
0 & 0 & 0 & e_{14}(z) & e_{15}(z) & 0 & \epsilon_{11}(z) & \epsilon_{12}(z) & 0 & d_{11}(z) & d_{12}(z) & 0 \\
0 & 0 & 0 & e_{24}(z) & e_{25}(z) & 0 & \epsilon_{12}(z) & \epsilon_{22}(z) & 0 & d_{12}(z) & d_{22}(z) & 0 \\
e_{31}(z) & e_{32}(z) & e_{33}(z) & 0 & 0 & 0 & 0 & 0 & \epsilon_{33}(z) & 0 & 0 & d_{33}(z) \\
\hline
0 & 0 & 0 & q_{14}(z) & q_{15}(z) & 0 & d_{11}(z) & d_{12}(z) & 0 & \mu_{11}(z) & \mu_{12}(z) & 0 \\
0 & 0 & 0 & q_{24}(z) & q_{25}(z) & 0 & d_{12}(z) & d_{22}(z) & 0 & \mu_{12}(z) & \mu_{22}(z) & 0 \\
q_{31}(z) & q_{32}(z) & q_{33}(z) & 0 & 0 & 0 & 0 & 0 & d_{33}(z) & 0 & 0 & \mu_{33}(z)
\end{array}\right] . \tag{4}$$

The specific values for the different material properties are given in Table 1.

The components of strain, electric field, and magnetic field are related to the displacement field u_i, and the electric and magnetic potentials ϕ and ψ by the relations

$$S_{ij} = \frac{1}{2}\left(\frac{\partial u_i}{\partial x_j} + \frac{\partial u_j}{\partial x_i}\right) \tag{5}$$

$$E_i = -\phi_{,i} \tag{6}$$

TABLE 1
Material properties

Parameter	Aluminum	Zirconia	Material A	Graphite-Epoxy	$CoFe_2O_4$	$BaTiO_3$
C_{11} (GPa)	94.2307	256.5052	7.3801	183.443	286.0	166.0
C_{22}	94.2307	256.5052	1.7341	11.662	286.0	166.0
C_{33}	94.2307	256.5052	7.3802	11.662	269.5	162.0
C_{13}	40.3846	109.3889	3.4450	4.363	170.5	78.0
C_{23}	40.3846	109.3889	1.3780	3.918	170.5	78.0
C_{12}	40.3846	109.3889	3.4450	4.363	173.0	77.0
C_{44}	26.9231	73.5582	2.3121	2.870	45.3	43.0
C_{55}	26.9231	73.5582	1.8682	7.170	45.3	43.0
C_{66}	26.9231	73.5582	2.3121	7.170	56.5	44.5
e_{31} (C/m^2)	NA	NA	NA	NA	0.0	−4.4
e_{32}	NA	NA	NA	NA	0.0	−4.4
e_{33}	NA	NA	NA	NA	0.0	18.6
e_{24}	NA	NA	NA	NA	0.0	11.6
e_{15}	NA	NA	NA	NA	0.0	11.6
q_{31} (N/Am)	NA	NA	NA	NA	580.3	0.0
q_{32}	NA	NA	NA	NA	580.3	0.0
q_{33}	NA	NA	NA	NA	699.7	0.0
q_{24}	NA	NA	NA	NA	550.0	0.0
q_{15}	NA	NA	NA	NA	550.0	0.0
ϵ_{11} (10^{-9}C^2/Nm^2)	NA	NA	NA	NA	0.080	11.2
ϵ_{22}	NA	NA	NA	NA	0.080	11.2
ϵ_{33}	NA	NA	NA	NA	0.093	12.6
$d_{11} = d_{22} = d_{33}$	NA	NA	NA	NA	0.0	0.0
μ_{11} (10^{-6}Ns^2/C^{2}2)	NA	NA	NA	NA	−590.0	5.0
μ_{22}	NA	NA	NA	NA	−590.0	5.0
μ_{33}	NA	NA	NA	NA	157.0	10.0
ρ (kg/m^3)	2702.0	5700.0	1.0	1590.0	5300.0	5800.0

$$H_i = -\psi_{,i} \quad (7)$$

where the subscript $_{,i}$ denotes partial differentiation with respect to x_i.

The equations of motion and the Gauss's laws for electrostatics and magnetism, and assuming absence of body force, free charge density, and free current density are given as

$$\sigma_{ij,j} = \rho(z)u_{i,tt} \quad (8)$$

$$D_{i,i} = 0 \quad (9)$$

$$B_{i,i} = 0 \quad (10)$$

where t and $\rho(z)$ are time and material mass density respectively.

2.3. Variational Formulation

Following the standard variational method of approximation (see Reddy [32]), we multiply each of the three governing equations by the first variation of the displacements, electric and magnetic potential respectively, we then integrate the result over the volume of the domain and set the result equal to zero, resulting in

$$\int_V \delta u_i(\sigma_{ij,j} - \rho(z)u_{i,tt})dV = 0 \quad (11)$$

$$\int_V \delta\phi(D_{i,i})dV = 0 \quad (12)$$

$$\int_V \delta\psi(B_{i,i})dV = 0 \quad (13)$$

Integrating this equations by parts and applying the divergence theorem yields the final weak form of the governing equations and they represent the principle of virtual work in the absence of body forces.

$$0 = \int_V (\sigma_{ij}\delta\gamma_{ij} + \delta u_i \rho(z)u_{i,tt})dV - \oint_S \sigma_{ij}n_j\delta u_i dS \quad (14)$$

$$0 = \int_V D_j\delta\phi_{,j}dV - \oint_S D_j n_j \delta\phi dS \quad (15)$$

$$0 = \int_V B_j\delta\psi_{,j}dV - \oint_S B_j n_j \delta\psi dS \quad (16)$$

Substituting the constitutive equations into the final weak form yields the following expressions that include the transition functions describing the through-thickness variation of the components of the material property tensors:

$$
\begin{aligned}
0 = \int_V \Bigg\{ & \Bigg[C_{11}(z)\frac{\partial u}{\partial x} + C_{12}(z)\frac{\partial v}{\partial y} + C_{13}(z)\frac{\partial w}{\partial z} \\
& + C_{16}(z)\left(\frac{\partial u}{\partial y} + \frac{\partial v}{\partial x}\right) + e_{31}(z)\frac{\partial \phi}{\partial z} q_{31}(z)\frac{\partial \psi}{\partial z} \Bigg] \frac{\partial \delta u}{\partial x} \\
& + \Bigg[C_{12}(z)\frac{\partial u}{\partial x} + C_{22}(z)\frac{\partial v}{\partial y} + C_{23}(z)\frac{\partial w}{\partial z} + C_{26}(z)\left(\frac{\partial u}{\partial y} + \frac{\partial v}{\partial x}\right) \\
& + e_{32}(z)\frac{\partial \phi}{\partial z} + q_{32}(z)\frac{\partial \psi}{\partial z} \Bigg] \frac{\partial \delta v}{\partial y} + \Bigg[C_{13}(z)\frac{\partial u}{\partial x} + C_{23}(z)\frac{\partial v}{\partial y} \\
& + C_{33}(z)\frac{\partial w}{\partial z} + C_{36}(z)\left(\frac{\partial u}{\partial y} + \frac{\partial v}{\partial x}\right) + e_{33}(z)\frac{\partial \phi}{\partial z} + q_{33}(z)\frac{\partial \psi}{\partial z} \Bigg] \\
& \times \frac{\partial \delta w}{\partial z} + \Bigg[C_{44}(z)\left(\frac{\partial v}{\partial z} + \frac{\partial w}{\partial y}\right) + C_{45}(z)\left(\frac{\partial u}{\partial z} + \frac{\partial w}{\partial x}\right) + \\
& e_{14}(z)\frac{\partial \phi}{\partial x} + e_{24}(z)\frac{\partial \phi}{\partial y} + q_{14}(z)\frac{\partial \psi}{\partial x} + q_{24}(z)\frac{\partial \psi}{\partial y} \Bigg] \\
& \times \left(\frac{\partial \delta v}{\partial z} + \frac{\partial \delta w}{\partial y}\right) + \Bigg[C_{45}(z)\left(\frac{\partial v}{\partial z} + \frac{\partial w}{\partial y}\right) \\
& + C_{55}(z)\left(\frac{\partial u}{\partial z} + \frac{\partial w}{\partial x}\right) + e_{15}(z)\frac{\partial \phi}{\partial x} + e_{25}(z)\frac{\partial \phi}{\partial y} + q_{15}(z)\frac{\partial \psi}{\partial x} \\
& + q_{25}(z)\frac{\partial \psi}{\partial y} \Bigg] \left(\frac{\partial \delta u}{\partial z} + \frac{\partial \delta w}{\partial x}\right) + \Bigg[C_{16}(z)\frac{\partial u}{\partial x} + C_{26}(z)\frac{\partial v}{\partial y} \\
& + C_{36}(z)\frac{\partial w}{\partial z} + C_{66}(z)\left(\frac{\partial u}{\partial y} + \frac{\partial v}{\partial x}\right) \Bigg] \left(\frac{\partial \delta u}{\partial y} + \frac{\partial \delta v}{\partial x}\right) - \\
& + \rho(z)\left(\frac{\partial^2 u}{\partial t^2}\delta u + \frac{\partial^2 v}{\partial t^2}\delta v + \frac{\partial^2 z}{\partial t^2}\delta w\right) \Bigg\} dV \\
& - \oint_S (t_x \delta u + t_y \delta v + t_z \delta z) dS
\end{aligned} \tag{17}
$$

$$
\begin{aligned}
0 = \int_V \Bigg\{ & \Bigg[e_{14}(z)\left(\frac{\partial v}{\partial z} + \frac{\partial w}{\partial y}\right) + e_{15}(z)\left(\frac{\partial u}{\partial z} + \frac{\partial w}{\partial x}\right) \\
& - \epsilon_{11}(z)\frac{\partial \phi}{\partial x} - \epsilon_{12}(z)\frac{\partial \phi}{\partial y} - d_{11}(z)\frac{\partial \psi}{\partial x} - d_{12}(z)\frac{\partial \psi}{\partial y} \Bigg] \frac{\partial \delta \phi}{\partial x} \\
& + \Bigg[e_{24}(z)\left(\frac{\partial v}{\partial z} + \frac{\partial w}{\partial y}\right) + e_{25}(z)\left(\frac{\partial u}{\partial z} + \frac{\partial w}{\partial x}\right) - \epsilon_{12}(z)\frac{\partial \phi}{\partial x} \\
& - \epsilon_{22}(z)\frac{\partial \phi}{\partial y} - d_{12}(z)\frac{\partial \psi}{\partial x} - d_{22}(z)\frac{\partial \psi}{\partial y} \Bigg] \frac{\partial \delta \phi}{\partial y} + \Bigg[e_{31}(z)\frac{\partial u}{\partial x} \\
& + e_{32}(z)\frac{\partial v}{\partial y} + e_{33}(z)\frac{\partial w}{\partial z} - \epsilon_{33}(z)\frac{\partial \phi}{\partial z} - d_{33}(z)\frac{\partial \psi}{\partial z} \Bigg] \frac{\partial \delta \phi}{\partial z} \Bigg\} dV \\
& - \oint_S D_j n_j \delta \phi dS
\end{aligned} \tag{18}
$$

$$
\begin{aligned}
0 = \int_V \Bigg\{ & \Bigg[q_{14}(z)\left(\frac{\partial v}{\partial z} + \frac{\partial w}{\partial y}\right) + q_{15}(z)\left(\frac{\partial u}{\partial z} + \frac{\partial w}{\partial x}\right) \\
& - d_{11}(z)\frac{\partial \phi}{\partial x} - d_{12}(z)\frac{\partial \phi}{\partial y} - \mu_{11}(z)\frac{\partial \psi}{\partial x} - \mu_{12}(z)\frac{\partial \psi}{\partial y} \Bigg] \frac{\partial \delta \psi}{\partial x} \\
& + \Bigg[q_{24}(z)\left(\frac{\partial v}{\partial z} + \frac{\partial w}{\partial y}\right) + q_{25}(z)\left(\frac{\partial u}{\partial z} + \frac{\partial w}{\partial x}\right) - d_{12}(z)\frac{\partial \phi}{\partial x} \\
& - d_{22}(z)\frac{\partial \phi}{\partial y} - \mu_{12}(z)\frac{\partial \psi}{\partial x} - \mu_{22}(z)\frac{\partial \psi}{\partial y} \Bigg] \frac{\partial \delta \psi}{\partial y} + \Bigg[q_{31}(z)\frac{\partial u}{\partial x} \\
& + q_{32}(z)\frac{\partial v}{\partial y} + q_{33}(z)\frac{\partial w}{\partial z} - d_{33}(z)\frac{\partial \phi}{\partial z} - \mu_{33}(z)\frac{\partial \psi}{\partial z} \Bigg] \frac{\partial \delta \psi}{\partial z} \Bigg\} dV \\
& - \oint_S B_j n_j \delta \psi dS
\end{aligned} \tag{19}
$$

where u, v, and w represent the displacement components in the x, y, and z directions respectively, and t_x, t_y, and t_z the traction components. Note that Eq. (17) results in three independent equations of equilibrium when the coefficients of the variations of the displacements are collected.

2.4. Discrete-Layer Approximation and Solution

The displacements u_i, the electric potential ϕ, and the magnetic potential ψ are approximated by a finite linear combination of functions that must satisfy the boundary conditions and be continuous as required by the variational principle. Approximations to the three displacements and two potentials are developed in terms of the global (x, y, z) coordinates. These approximations are constructed in such a way as to separate the dependence in the plane of the plate with that in the direction perpendicular to the interface. Hence approximations for the five principal unknowns are sought in the form

$$
\begin{aligned}
u(x, y, z) &= \sum_{i=1}^{m}\sum_{j=1}^{n} U_{ij}\Gamma_i^u(x, y)\varphi_j^u(z) \\
v(x, y, z) &= \sum_{i=1}^{m}\sum_{j=1}^{n} V_{ij}\Gamma_i^v(x, y)\varphi_j^v(z) \\
w(x, y, z) &= \sum_{i=1}^{m}\sum_{j=1}^{n} W_{ij}\Gamma_i^w(x, y)\varphi_j^w(z) \\
\phi(x, y, z) &= \sum_{i=1}^{m}\sum_{j=1}^{n} \Phi_{ij}\Gamma_i^\phi(x, y)\varphi_j^\phi(z) \\
\psi(x, y, z) &= \sum_{i=1}^{m}\sum_{j=1}^{n} \Psi_{ij}\Gamma_i^\psi(x, y)\varphi_j^\psi(z)
\end{aligned} \tag{20}
$$

where, the elements U_{ij}, V_{ij}, W_{ij}, Ψ_{ij}, and Φ_{ij} are the approximation coefficients associated with the jth layer of the discretized laminate corresponding to the ith term of the in-plane approximation function for the displacement and potential variables respectively. In the thickness direction, one-dimensional Lagrangian interpolation polynomials are used for $\varphi_j(z)$ for each variable, while for the in-plane functions $\Gamma_i(x, y)$, different types of approximations can be used being power and Fourier series the most commonly selected.

Substitution of these approximation functions into Eqs. (17), (18) and (19), collecting the coefficients of the variations of

the displacements and potentials, integrating with respect to the thickness coordinate z, and placing the results in matrix form yields the result

$$\begin{bmatrix} [M^{uu}] & [0] & [0] & [0] & [0] \\ [0] & [M^{vv}] & [0] & [0] & [0] \\ [0] & [0] & [M^{ww}] & [0] & [0] \\ [0] & [0] & [0] & [0] & [0] \\ [0] & [0] & [0] & [0] & [0] \end{bmatrix} \begin{Bmatrix} \{\ddot{u}\} \\ \{\ddot{v}\} \\ \{\ddot{w}\} \\ \{0\} \\ \{0\} \end{Bmatrix} + \begin{bmatrix} [K^{uu}] & [K^{uv}] & [K^{uw}] & [K^{u\phi}] & [K^{u\psi}] \\ [K^{vu}] & [K^{vv}] & [K^{vw}] & [K^{v\phi}] & [K^{v\psi}] \\ [K^{wu}] & [K^{wv}] & [K^{ww}] & [K^{w\phi}] & [K^{w\psi}] \\ [K^{\phi u}] & [K^{\phi v}] & [K^{\phi w}] & [K^{\phi\phi}] & [K^{\phi\psi}] \\ [K^{\psi u}] & [K^{\psi v}] & [K^{\psi w}] & [K^{\psi\phi}] & [K^{\psi\psi}] \end{bmatrix} \begin{Bmatrix} \{u\} \\ \{v\} \\ \{w\} \\ \{\phi\} \\ \{\psi\} \end{Bmatrix} = \begin{Bmatrix} \{f^u\} \\ \{f^v\} \\ \{f^w\} \\ \{f^\phi\} \\ \{f^\psi\} \end{Bmatrix} \tag{21}$$

where the sub-matrices $[K]$ contain the elements of the stiffness matrix, the sub-matrices $[M]$ represent the mass associated with each displacement, the vectors $\{u\}$, $\{v\}$, $\{w\}$, $\{\psi\}$, and $\{\phi\}$ are the corresponding approximation coefficients U_{ij}, V_{ij}, W_{ij}, Ψ_{ij}, and Φ_{ij} of Eq. (20), and the vectors $\{f^u\}$, $\{f^v\}$, $\{f^w\}$, $\{f^\psi\}$, and $\{f^\phi\}$ represent the external loading and potentials acting on the plate.

The dynamic analysis of the laminates is developed assuming harmonic motion. Therefore, the solutions for the primary unknowns have the form

$$u_i(x, y, z, t) = u_i(x, y, z)e^{i\omega t} \tag{22}$$

$$\phi(x, y, z, t) = \phi(x, y, z)e^{i\omega t} \tag{23}$$

$$\psi(x, y, z, t) = \psi(x, y, z)e^{i\omega t} \tag{24}$$

where ω is the natural frequency.

Taking second derivative with respect to time of Eq. (22) gives

$$\ddot{u}_i(x, y, z, t) = -\omega^2 u_i(x, y, z)e^{i\omega t} \tag{25}$$

Replacing Eqs. (23) to (25) into Eq. (21), and simplifying the dynamic problem becomes the following eigenvalue problem:

$$\begin{bmatrix} [K^{uu}] & [K^{uv}] & [K^{uw}] & [K^{u\phi}] & [K^{u\psi}] \\ [K^{vu}] & [K^{vv}] & [K^{vw}] & [K^{v\phi}] & [K^{v\psi}] \\ [K^{wu}] & [K^{wv}] & [K^{ww}] & [K^{w\phi}] & [K^{w\psi}] \\ [K^{\phi u}] & [K^{\phi v}] & [K^{\phi w}] & [K^{\phi\phi}] & [K^{\phi\psi}] \\ [K^{\psi u}] & [K^{\psi v}] & [K^{\psi w}] & [K^{\psi\phi}] & [K^{\psi\psi}] \end{bmatrix} \begin{Bmatrix} \{u\} \\ \{v\} \\ \{w\} \\ \{\phi\} \\ \{\psi\} \end{Bmatrix} - \omega^2 \begin{bmatrix} [M^{uu}] & [0] & [0] & [0] & [0] \\ [0] & [M^{vv}] & [0] & [0] & [0] \\ [0] & [0] & [M^{ww}] & [0] & [0] \\ [0] & [0] & [0] & [0] & [0] \\ [0] & [0] & [0] & [0] & [0] \end{bmatrix} \begin{Bmatrix} \{u\} \\ \{v\} \\ \{w\} \\ \{0\} \\ \{0\} \end{Bmatrix} = \begin{Bmatrix} \{0\} \\ \{0\} \\ \{0\} \\ \{0\} \\ \{0\} \end{Bmatrix} \tag{26}$$

The natural frequencies and the corresponding shape functions can be found by solving this eigenvalue problem with no external forces since free vibration analysis is assumed. The electric and magnetic potentials are eliminated from this equation by following a standard matrix condensation procedure, allowing solution by using direct eigensolvers. First we consider the following partition of the matrix Eq. (26)

$$\begin{bmatrix} [K^{UU}] & [K^{U\Phi}] \\ [K^{\Phi U}] & [K^{\Phi\Phi}] \end{bmatrix} \begin{Bmatrix} \{U\} \\ \{\Phi\} \end{Bmatrix} - \omega^2 \begin{bmatrix} [M^{UU}] & [0] \\ [0] & [0] \end{bmatrix} \begin{Bmatrix} \{U\} \\ \{0\} \end{Bmatrix} = \begin{Bmatrix} \{0\} \\ \{0\} \end{Bmatrix} \tag{27}$$

expanding Eq. (27) gives the matrix equations

$$[K^{UU}]\{U\} + [K^{U\Phi}]\{\Phi\} - \omega^2[M^{UU}]\{U\} = \{0\} \tag{28}$$

$$[K^{\Phi U}]\{U\} + [K^{\Phi\Phi}]\{\Phi\} = \{0\} \tag{29}$$

Solving for Φ from Eq. (29) and substituting back in Eq. (27) results in the following general eigenvalue problem

$$([\bar{K}] - \omega^2[M])\{U\} = \{0\} \tag{30}$$

where U represents the modes shapes, ω is the natural frequency, and the condensed stiffness matrix $[\bar{K}]$ is calculated as

$$[\bar{K}] = ([K^{UU}] - [K^{U\Phi}][K^{\Phi\Phi}]^{-1}[K^{\Phi U}]) \tag{31}$$

The elements of each of the sub-matrices $[K]$ and $[M]$ in Eq. (26) have a specific form as a result of the pre-integration with respect to the thickness coordinate. They consist of the product of the thickness approximation functions and the gradient function representing the through-thickness variation of the material properties, fully integrated, and then multiplied by the in-plane approximations.

In order to illustrate the pre-integration with respect to the thickness coordinate, we consider the sub-matrix $[K^{uu}]$ given by

$$K^{uu} = \int_V \left[C_{11}(z)\frac{\partial u}{\partial x}\frac{\partial u}{\partial x} + C_{16}(z)\left(\frac{\partial u}{\partial y}\frac{\partial u}{\partial x} + \frac{\partial u}{\partial x}\frac{\partial u}{\partial y}\right) + C_{55}(z)\frac{\partial u}{\partial z}\frac{\partial u}{\partial z} + C_{66}(z)\frac{\partial u}{\partial y}\frac{\partial u}{\partial y}\right] dV \tag{32}$$

Substituting the approximation functions (20) in Eq. (32), its first term becomes

$$\int_V C_{11}(z)\left(\sum_{i=1}^{m}\sum_{\alpha=1}^{N+1}\frac{\partial \Gamma_i^u(x, y)}{\partial x}\varphi_\alpha^u(z)\right) \times \left(\sum_{j=1}^{m}\sum_{\beta=1}^{N+1}\frac{\partial \Gamma_j^u(x, y)}{\partial x}\varphi_\beta^u(z)\right) dV \tag{33}$$

where, m is the number of terms in the in-plane approximation functions, and N is the total number of layers in the laminate. The summations for α and β extend to $(N+1)$ which is the number of layer interfaces in the laminated plate and the number of approximation functions in the thickness direction. Expression (33) can be re-written as

$$\int_0^H C_{11}(z) \sum_{\alpha=1}^{N+1} \sum_{\beta=1}^{N+1} \varphi_\alpha^u(z)\varphi_\beta^u(z)dz \int_0^{L_x} \times \int_0^{L_y} \sum_{i=1}^{m} \sum_{j=1}^{m} \frac{\partial \Gamma_i^u(x,y)}{\partial x} \frac{\partial \Gamma_j^u(x,y)}{\partial x} dxdy \quad (34)$$

and with the first integral termed as $A_{\alpha\beta}$, expression (34) can be written as

$$A_{\alpha\beta} \int_0^{L_x} \int_0^{L_y} \sum_{i=1}^{m} \sum_{j=1}^{m} \frac{\partial \Gamma_i^u(x,y)}{\partial x} \frac{\partial \Gamma_j^u(x,y)}{\partial x} dxdy \quad (35)$$

The linear Lagrangian interpolation functions used in the thickness direction are defined as [33]

$$\varphi_1(z) = 1 - \frac{z - z_1}{z_2 - z_1} \quad z_1 \le z \le z_2 \quad (36)$$

$$\varphi_k(z) = \frac{z - z_{k-1}}{z_k - z_{k-1}} \quad z_{k-1} \le z \le z_k \quad (37)$$

$$\varphi_k(z) = 1 - \frac{z - z_k}{z_{k+1} - z_k} \quad z_k \le z \le z_{k+1} \quad (38)$$

$$\varphi_{N+1}(z) = \frac{z - z_n}{z_{n+1} - z_n} \quad z_n \le z \le z_{n+1} \quad (39)$$

where z_k are the coordinates of the top and bottom surfaces of each discrete layer. Note that the sum over the number of layers of the laminate in expression (34) is limited to the layers over which the functions $\varphi_k(z)$ are defined. These functions are defined at the most over two adjacent layers [34].

Substituting equations (36)–(39) into expression (35), the first element of the matrix $A_{\alpha\beta}$ is given by

$$A_{11} = \int_{z_1}^{z_2} C_{11}(z)\left(1 - \frac{z - z_1}{z_2 - z_1}\right)^2 dz \quad (40)$$

where, z_1 and z_2 are the thickness coordinates of the bottom and top surfaces respectively of the corresponding layer. It is important to realize that the form of the pre-integrated elements of the sub-matrices depends on the transition function describing the gradient of the material properties through the thickness of the laminate. Furthermore, any continuous transition function may be implemented in the present discrete layer approach. Neither the pre-integration in the thickness direction nor the inclusion of the gradation function into the governing equations alters the symmetry of the global stiffness matrix.

3. NUMERICAL EXAMPLES

Four different examples are considered in this section. First, the solution is validated by determining the natural frequencies of a simply supported functionally graded square plate made of a composite material obtained by mixing a metal (Aluminum) and a ceramic (Zirconia) material. The effective properties are determined by using the Mori-Tanaka scheme, and results are compared to the exact solutions published by Vel and Batra [19]. Natural frequencies of rectangular plates made of Aluminum/Zirconia are also determined. Then, three more examples are considered: an elastic composite plate in which the material properties exhibit an exponential variation through the thickness of the laminate, a plate made of an orthotropic fiber reinforced material (Graphite/Epoxy) with the in-plane orientation of the fibers gradually varying as a function of the z coordinate, and finally, the natural frequencies of a two-material magneto-electro-elastic composite plate made of a piezoelectric material ($BaTiO_3$), and a magnetostrictive material ($CoFe_2O_4$) are determined considering that the volume fraction of the constituents continuously changes through the thickness of the plate. Through-thickness variations of some of the material properties for each type of gradation are shown in Figure 1.

Each numerical example is solved using two different approaches. First, the functions describing the gradation of the corresponding material property are incorporated into the governing equations and analytically or numerically integrated before assembling the stiffness and mass matrices, and before solving the eigenvalue problem. In a second approach, the plates are discretized into a finite number of homogenous layers with material properties determined by the average values within the respective layer and according to the corresponding gradation function, that is

$$\bar{P}_{ik} = \int_{z_1}^{z_2} \frac{P_{ik}(z)}{z_2 - z_1} dz \quad (41)$$

where P represents any material property, and z_1 and z_2 are the coordinates of the bottom and top surfaces of the respective layer. Specializing the previous equation for the first component of the elastic tensor, and after substituting back in Eq. (40) the first element of the matrix $A_{\alpha\beta}$ becomes

$$A_{11} = \int_{z_1}^{z_2} \bar{C}_{11}\left(1 - \frac{z - z_1}{z_2 - z_1}\right)^2 dz = \bar{C}_{11}\frac{z_2 - z_1}{3} \quad (42)$$

These two approaches are considered in order to evaluate the need for including the gradation functions into the governing equilibrium equations.

Normalized natural frequencies are shown in Tables 2–11 for the different examples presented in this paper. Frequencies obtained considering gradation functions (Approach 1) are shown in columns with the heading "Graded," while the columns named "Homog" show frequencies determined using homogeneous discrete layers (Approach 2). The natural frequencies are

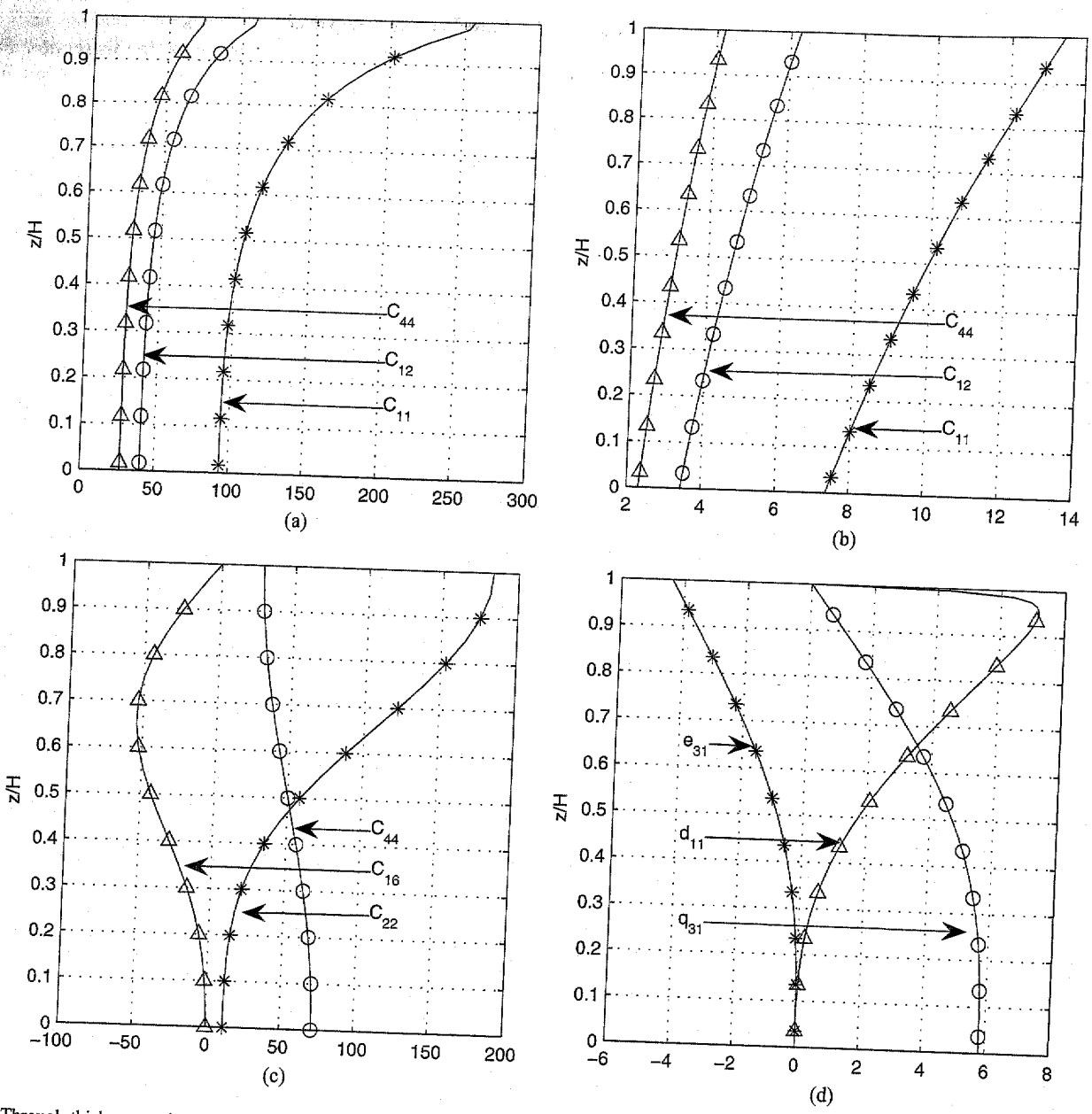

FIG. 1. Through-thickness variation of material properties for $\eta = 3$: a. Al/ZrO_2, b. Exponential Material, c. Graphite/Epoxy, and d. $BatiO_3/CoFe_2O_4$. (C_{ij} in GPa, except for C_{44} in $10 \times$ GPa in part 1c., e_{ij} in C/m^2, q_{ij} in $10^2 \times$ N/Am, and d_{ij} in $10^{-12} \times$ Ns/VC).

normalized as

$$\bar{\omega}_n = \omega_n (L_x^2/H)\sqrt{(\rho/C_{11})} \tag{43}$$

where ρ and C_{11} are the effective mass density and the corresponding element of the effective elastic stiffness matrix of the composite material at the bottom of the plate.

To show the applicability of the present model, all the plates considered here are analyzed for two different boundary conditions: four edges simply-supported (SSSS), and two opposite edges simply supported at $x = 0$ and $x = L_x$, and the other two free at $y = 0$ and $y = L_y$ (SFSF).

The natural frequencies are first determined for plates with its four edges simply supported (SSSS). The edge boundary conditions are consistent with those of simple support. Hence, the transverse displacement w is specified to be zero, with zero electric and magnetic potential (when applicable), and zero normal traction also specified along the edge length and along the top and bottom surfaces of the laminate. These tractions appear in Eqs. (14) and (17) as natural boundary conditions, and the free condition is satisfied in the present approach only in an integral sense and not pointwise as in exact solutions. The in-plane approximation functions for each of the three displacements and two potentials are given in the

TABLE 2
Comparison of normalized natural frequencies of a simply supported square Al/ZrO_2 plate with $\eta = 1$

	$H/L_x = 0.05$		$H/L_x = 0.10$		$H/L_x = 0.20$	
	Exact	Present	Exact	Present	Exact	Present
1	6.120	6.120	5.960	5.960	5.480	5.478
2	58.240	58.200	29.120	29.100	14.733	14.550
3	98.160	98.080	49.010	48.980	24.380	24.365
4	823.920	823.720	207.500	207.450	53.390	53.353

form:

$$\Gamma_j^u(x, y) = \cos px \sin qy \tag{44}$$

$$\Gamma_j^v(x, y) = \sin px \cos qy \tag{45}$$

$$\Gamma_j^w(x, y) = \sin px \sin py \tag{46}$$

$$\Gamma_j^\phi(x, y) = \sin px \sin qy \tag{47}$$

$$\Gamma_j^\psi(x, y) = \sin px \sin py \tag{48}$$

where $p = n\pi/L_x$ and $q = m\pi/L_x$. Here the index j is a single integer that is linked to the numbers used for p and q in each of the terms of the approximation functions. For the simply supported boundary conditions considered in these examples only one term is required to match the exact solution corresponding to the first axial mode (i.e., $p = 1$, $q = 1$). The plate is discretized into an increasing number of layers until convergence is achieved for both thickness representation approaches when 30 layers are used.

For the SFSF cases, the plate is simply supported along two opposite edges at $x = 0$ and $x = L_x$, and the other two edges at $y = 0$ and $y = L_y$ are free. The traction free conditions at the top and bottom surfaces are the same as in the previous example. To satisfy the support conditions, power series are used for the approximation functions of the three displacements, electric and magnetic potentials. The approximation functions for the displacements satisfy the essential boundary conditions because they do not enforce zero displacement at the free edges, but they do at simply supported edges. They are given by

$$\Gamma_j^u(x, y) = (x - L_x/2)^n [y(y - L_y)]^{(m+1)} \quad n, m = 0, 1, 2, 3, \ldots \tag{49}$$

$$\Gamma_j^v(x, y) = [x(x - L_x)]^{(n+1)} (y - L_y/2)^m \quad n, m = 0, 1, 2, 3, \ldots \tag{50}$$

$$\Gamma_j^w(x, y) = (x - L_x/2)^n [y(y - L_y)]^{(m+1)} \quad n, m = 0, 1, 2, 3, \ldots \tag{51}$$

$$\Gamma_j^\phi(x, y) = \sin px \sin qy \tag{52}$$

$$\Gamma_j^\psi(x, y) = \sin px \sin py \tag{53}$$

Analyses are performed for an increasing number of layers and terms in these approximation functions, achieving convergence for both approaches with 30 layers and $m = n = 7$.

The length of the square plate in the validation example is 1.0 m, with three different aspect ratios $H/L_x = 0.05, 0.10$, and 0.20 being considered. The geometry of the plates used in the remaining examples is the same, that is, the length $L_x = 2.0$ m, the width $L_y = 1.0$ m, and two thickness to length ratios are studied $H/L_x = 0.1$ and $H/L_x = 0.20$. The properties of the material constituents of the plates are shown in Table 1.

3.1. Aluminum-Zirconia Composite Graded Plates

The first example considers a metal-ceramic composite plate made of two isotropic component materials, aluminum (Al) and Zirconia (ZrO_2) with material properties shown in Table 1. The variation of the volume fraction of the ceramic phase V_c, and of the metal phase V_m as functions of the thickness coordinate are given by

$$V_c(z) = \left(\frac{z}{H}\right)^\eta \tag{54}$$

$$V_m(z) = 1 - V_c(z) \tag{55}$$

Here, η is a parameter determining the ceramic volume fraction variation through the thickness of the plate. Four different η values (1, 2, 3 and 5), are considered for the square plate, while for the rectangular plates only two values $\eta = 1$ and $\eta = 3$ are considered . At the bottom of the plate ($z = 0$) the volume fraction of the ceramic is zero, while it is 1.0 at the top of the plate ($z = H$).

The gradation functions describing the variation of the effective material properties at any height z within the plate are determined as a function of the volume fraction of the ceramic phase. The latter is done by using the Mori-Tanaka scheme assuming a graded material having a well defined matrix (Al) reinforced by spherical particles of the particulate phase (ZrO_2) [19, 22]. As a result, the effective material properties are expressed as

$$\rho(z) = \rho_c V_c(z) + \rho_m V_m(z) \tag{56}$$

$$K(z) = \frac{V_c(z)(K_c - K_m)}{\left(1 + (1 - V_c(z))\frac{K_c - K_m}{K_m + (4/3)\mu_m}\right)} + K_m \tag{57}$$

$$\mu(z) = \frac{V_c(z)(\mu_c - \mu_m)}{\left(1 + (1 - V_c(z))\frac{\mu_c - \mu_m}{\mu_c + f_m}\right)} + \mu_m \tag{58}$$

$$f_m = \mu_m \frac{9K_m + 8\mu_m}{6(K_m + 2\mu_M)} \tag{59}$$

$$\lambda(z) = K(z) - 2\mu/3 \tag{60}$$

where $K(z)$, K_c, and K_m are the bulk moduli of the composite, ceramic, and metal materials respectively, $\mu(z)$, μ_c, and μ_m are the shear moduli, and $\lambda(z)$, λ_c, and λ_m are the corresponding Lamé constants. Through-thickness variation of the engineering

TABLE 3
Comparison of normalized natural frequencies of a simply supported square Al/ZrO_2 plate with $H/L_x = 0.20$

	$\eta = 2$		$\eta = 3$		$\eta = 5$	
	Exact	Present	Exact	Present	Exact	Present
1	5.493	5.490	5.528	5.528	5.563	5.563
2	14.278	14.270	14.150	14.145	14.025	14.023
3	23.910	23.898	23.695	23.688	23.495	23.488
4	50.375	50.373	48.825	48.823	47.688	47.688

elastic constants are shown in Figure 1a, and they are calculated as

$$C_{11}(z) = C_{22}(z) = C_{33}(z) = \lambda(z) + 2\mu(z) \tag{61}$$

$$C_{44}(z) = C_{55}(z) = C_{66}(z) = \mu(z) \tag{62}$$

$$C_{23}(z) = C_{13}(z) = C_{12}(z) = \lambda(z) \tag{63}$$

Substitution of Eqs. (56) to (63) into Eq. (40) results in the first component of the matrix $A_{\alpha\beta}$ that represents the pre-integration with respect to the thickness coordinate, and is given by

$$A_{11} = \int_{z_1}^{z_2} \left[\frac{\left(\frac{z}{H}\right)^{\eta}(K_c - K_m)}{\left(1 + \left(1 - \left(\frac{z}{H}\right)^{\eta}\right)\frac{K_c - K_m}{K_m + (4/3)\mu_m}\right)} + K_m + \frac{\left(\frac{z}{H}\right)^{\eta}(\mu_c - \mu_m)}{\left(1 + \left(1 - \left(\frac{z}{H}\right)^{\eta}\right)\frac{\mu_c - \mu_m}{\mu_c + f_m}\right)} + \mu_m \right] \left(1 - \frac{z - z_1}{z_2 - z_1}\right)^2 dz \tag{64}$$

These expressions are numerically integrated using 16 Gauss points within the computer code before assembling the stiffness and mass matrices, and before solving the eigenvalue problem.

Normalized natural frequencies for simply supported square plates are shown and compared to the exact solution published by Vel and Batra [19] in Tables 2 and 3. These values were extracted from Qian et al. [22] because of the presence of typographical errors in the original publication [35]. Excellent agreement is obtained. The first 10 normalized natural frequencies obtained by the two solution approaches, different aspect ratios, and different η values mentioned before are shown in Table 4 for the SSSS rectangular plates, and in Table 5 for SFSF plates. It can be seen from these tables that the maximum difference in the natural frequencies between approaches 1 and 2 is only 0.04%. This indicates that for the present discrete layer method, the use of homogeneous layers rather than incorporating the gradation functions into the governing equations results in excellent levels of accuracy, with the corresponding saving in effort and computer time.

Natural frequencies are reduced when the variation of the ceramic volume fraction changes from linear ($\eta = 1$) to cubic ($\eta = 3$). The change is about 3.0–4.0% for the first three frequencies, close to 8.0% for frequencies 4 to 6, and back to 3.0–4.0% for frequencies 7 to 10. These variations are similar between simply supported plates with aspect ratios $H/L_x = 0.10$ and $H/L_x = 0.20$, while it is practically the same for plates having two simply supported edges and two free edges.

3.2. Exponentially Graded Plates

After validation of the proposed method, single-layer rectangular plates made of an elastic orthotropic material were studied. The components of the elastic stiffness tensor for the material considered in this example vary exponentially as a function of the thickness coordinate, and the mass density is assumed to be constant throughout the plate. The elastic constants are then

TABLE 4
Normalized natural frequencies of a simply supported rectangular Al/ZrO_2 plate with $L_x = 2.0$ m. and $L_y = 1.0$ m

	$H/L_x = 0.1$				$H/L_x = 0.2$			
	$\eta = 1$		$\eta = 3$		$\eta = 1$		$\eta = 3$	
	Graded	Homog.	Graded	Homog.	Graded	Homog.	Graded	Homog.
1	14.249	14.243	14.444	14.440	12.050	12.047	12.007	12.005
2	46.013	46.008	44.732	44.730	22.992	22.990	22.359	22.358
3	77.255	77.247	75.126	75.122	38.065	38.062	36.942	36.940
4	210.448	210.435	192.170	192.173	56.217	56.212	51.830	51.830
5	221.620	221.603	203.661	203.662	65.255	65.247	60.968	60.967
6	367.929	367.907	338.285	338.290	89.172	89.165	82.114	82.114
7	410.581	410.557	393.718	393.714	104.525	104.518	100.297	100.296
8	428.867	428.842	408.720	408.715	116.142	116.134	110.756	110.755
9	611.680	611.642	591.484	591.474	152.971	152.959	147.867	147.864
10	613.641	613.605	593.513	593.503	154.672	154.662	149.618	149.616

TABLE 5
Normalized natural frequencies of a rectangular Al/ZrO_2 plate with $L_x = 2.0$ m., $L_y = 1.0$ m, two opposite edges simply supported and the remaining two free

	$H/L_x = 0.1$				$H/L_x = 0.2$			
	$\eta = 1$		$\eta = 3$		$\eta = 1$		$\eta = 3$	
	Graded	Homog.	Graded	Homog.	Graded	Homog.	Graded	Homog.
1	177.654	177.598	171.261	171.197	44.413	44.400	42.815	42.799
2	197.199	197.061	195.208	195.207	49.300	49.265	48.802	48.802
3	213.895	213.856	206.395	206.336	53.474	53.464	51.599	51.584
4	302.256	302.125	287.134	287.113	75.564	75.531	71.784	71.778
5	359.555	359.474	332.030	332.012	89.889	89.869	83.007	83.003
6	405.428	405.279	391.671	391.642	101.357	101.320	97.918	97.911
7	417.383	417.325	397.138	397.124	104.346	104.331	99.285	99.281
8	451.543	451.357	443.138	443.125	112.886	112.839	110.785	110.781
9	461.563	461.396	444.323	444.275	115.391	115.349	111.081	111.069
10	502.275	502.092	484.204	484.156	125.569	125.523	121.051	121.039

given by

$$C_{ik}(z) = C^o_{ik} e^{\eta z} \tag{65}$$

where C_{ik} are the components of the stiffness tensor at any height z, C^o_{ik} are the components at $z = 0$ and shown in Table 1 [23], and η is the exponential factor characterizing the degree of the material gradient in the z-direction. Note that η has units $[1/L]$, and $\eta = 0$ corresponds to a homogeneous material [23].

Substitution of Eq. (65) into Eq. (40) and performing the integration gives the first component of the matrix $A_{\alpha\beta}$ as

$$A_{11} = \int_{z_1}^{z_2} C^o_{11} e^{\eta z} \left(1 - \frac{z - z_1}{z_2 - z_1}\right)^2 dz C^o_{11} = \left\{ \frac{[2\eta^2 z_2 z_1 - 2\eta(z_2 - z_1) - \eta^2(z_2^2 + z_1^2) - 2]e^{\eta z_1} + 2e^{\eta z_2}}{\eta^3 (z_1 - z_2)^2} \right\} \tag{66}$$

where, z_1 and z_2 are the thickness coordinates of the bottom and top surfaces, respectively, of the corresponding layer.

Natural frequencies for three different exponential factors $\eta = 0$, $\eta = 1$, and $\eta = 3$ are shown in Tables 6 and 7 for both aspect ratios and boundary conditions considered. Excellent agreement is again obtained between approaches 1 and 2, with a maximum difference of 0.30% for SSSS plates and only 0.005% for the SFSF plates. As expected, the natural frequencies for the graded plates are higher than those for the homogeneous plate ($\eta = 0$) because the stiffness of the plate is increased when positive exponential factors are used for this type of gradation (see Figure 1b).

The frequencies increased when the exponential parameter was increased from 1 to 3 for both boundary conditions and aspect ratios considered. The change is about 10–12% for

TABLE 6
Normalized natural frequencies of a rectangular simply supported plate with material properties exponentially varying through the thickness of the plate, and with $L_x = 2.0$ m., $L_y = 1.0$ m

	$H/L_x = 0.1$					$H/L_x = 0.2$				
	$\eta = 0$	$\eta = 1$		$\eta = 3$		$\eta = 0$	$\eta = 1$		$\eta = 3$	
	Homog.	Graded	Homog.	Graded	Homog.	Homog.	Graded	Homog.	Graded	Homog.
1	32.551	34.229	34.229	37.904	37.909	19.228	21.283	21.283	26.322	26.321
2	52.384	55.103	55.103	61.192	61.193	26.179	28.924	28.924	35.228	35.229
3	145.900	153.317	153.317	168.879	168.910	43.106	47.641	47.641	58.224	58.224
4	275.350	289.345	289.345	318.687	318.933	71.442	78.844	78.844	95.236	95.236
5	299.887	314.716	314.717	343.044	343.075	80.884	89.206	89.206	107.188	107.188
6	319.926	335.877	335.878	367.821	367.899	105.125	116.000	116.000	139.945	139.945
7	372.671	392.497	392.496	439.388	439.415	138.688	153.028	153.028	175.612	175.637
8	411.316	432.225	432.225	476.099	476.963	152.687	162.070	162.074	184.549	184.549
9	527.935	554.894	554.894	612.338	612.684	153.226	171.730	171.730	207.946	207.947
10	547.647	575.490	575.490	633.934	635.987	165.419	185.007	185.007	226.721	226.732

TABLE 7
Normalized natural frequencies of a rectangular plate with material properties exponentially varying through the thickness of the plate, and with $L_x = 2.0$ m., $L_y = 1.0$ m, two opposite edges simply supported and the remaining two free

	$H/L_x = 0.1$				$H/L_x = 0.2$				
	$\eta = 0$	$\eta = 1$		$\eta = 3$		$\eta = 0$	$\eta = 1$		$\eta = 3$	
	Homog.	Graded	Homog.	Graded	Homog.	Homog.	Graded	Homog.	Graded	Homog.
1	6.035	6.346	6.346	7.023	7.023	4.267	4.720	4.720	5.808	5.808
2	13.958	14.684	14.684	16.310	16.310	7.444	8.230	8.230	10.106	10.106
3	21.464	22.585	22.585	25.145	25.145	10.732	11.917	11.917	15.099	15.099
4	24.152	25.394	25.394	28.094	28.094	15.929	17.626	17.626	21.741	21.740
5	41.818	43.990	43.990	48.860	48.860	21.464	23.738	23.738	29.137	29.138
6	42.928	45.159	45.159	50.175	50.175	22.056	24.396	24.396	30.000	30.001
7	52.384	55.103	55.103	61.188	61.189	26.177	28.917	28.918	35.179	35.182
8	60.248	63.367	63.367	70.302	70.302	32.196	35.661	35.661	44.244	44.243
9	64.392	67.745	67.745	75.324	75.324	32.248	35.705	35.705	44.293	44.294
10	67.653	71.141	71.141	78.793	78.793	36.126	39.957	39.957	49.088	49.090

$H/L_x = 0.10$ and 20–25% for $H/L_x = 0.20$. In this case, for exponentially graded plates, the effect of the gradation parameter in the natural frequencies is considerably different depending on the aspect ratio of the plate.

3.3. Graphite-Epoxy Graded Plates

The next example considers the analyses of plates made of the orthotropic fiber reinforced graphite-epoxy. Here, the orientation of the fibers is assumed to smoothly vary as a function of the z-coordinate, being oriented in the x-direction on the bottom surface and in y-direction on the top surface of the laminate. The in-plane orientation of the fibers measured with respect to the x-axis is expressed as

$$\theta(z) = \frac{\pi}{2}\left(\frac{z}{H}\right)^{\eta} \tag{67}$$

where η is the parameter determining the type of variation of the fiber orientation through the thickness of the plate. Materials having this configuration can be manufactured by stacking thin layers having different orientations [21], noting that as the fiber orientation changes the elements C_{16}, C_{26}, C_{36}, and C_{45} of the elastic stiffness matrix become nonzero as shown in Figure 1c for C_{16}. The magnitude of the components of the elastic stiffness tensor can be obtained at any hight z by typical tensor transformations as shown in Appendix A. As an example, the first component of the elastic stiffness tensor as a function of the fiber orientation is given by

$$\begin{aligned} C_{11}(\theta) = {} & C_{11}^{o}\cos^4(\theta) + C_{22}^{o}\sin^4(\theta) \\ & + 2\sin^2(\theta)\cos^2(\theta)\left(C_{11}^{o} + 2C_{66}^{o}\right) \end{aligned} \tag{68}$$

with Eqs. (67) and (68) in (40) giving the first components of the matrix $A_{\alpha\beta}$ as

$$\begin{aligned} A_{11} = \int_{z_1}^{z_2} & \left\{ C_{11}^{o}\cos^4\left[\frac{\pi}{2}\left(\frac{z}{H}\right)^{n}\right] + C_{22}^{o}\sin^4\left[\frac{\pi}{2}\left(\frac{z}{H}\right)^{n}\right] \right. \\ & \left. + 2\sin^2\left[\frac{\pi}{2}\left(\frac{z}{H}\right)^{n}\right]\cos^2\left[\frac{\pi}{2}\left(\frac{z}{H}\right)^{n}\right]\left(C_{11}^{o} + 2C_{66}^{o}\right)\right\} \\ & \times \left(1 - \frac{z - z_1}{z_2 - z_1}\right)^2 dz \end{aligned} \tag{69}$$

These expressions are also numerically integrated before assembling the stiffness and mass matrices, and before solving the eigenvalue problem.

Homogeneous plates ($\eta = 0$) with the fibers parallel to the x coordinate axis, and linear and cubic variations of the fiber orientation are considered in these examples (i.e. $\eta = 1$ and $\eta = 3$). Normalized natural frequencies can be seen in Tables 8 and 9 for SSSS and SFSF plates, respectively. Once again excellent results are obtained using discrete homogeneous layers with a maximum difference of 0.05% between approaches 1 and 2. It can be seen, when comparing the homogeneous plate frequencies to those of graded plates, that for SSSS plates the first frequency decreased, while the other increased. This may be from the fact that the first mode shape is primarily bending about the y-axis in which bending stiffness is reduced with the change in fiber orientation. For the other frequencies, there is a higher influence of the y-axis and two-way bending stiffnesses which are being increased. For SFSF plates, the repeated frequencies of the homogenous case, indicating symmetrical vibration modes, disappear for the graded plates because the plates are no longer symmetric in z.

TABLE 8
Normalized natural frequencies of a rectangular simply supported Graphite/Epoxy plate with the orientation of the fibers continuously changing as a function of the thickness coordinate, and with $L_x = 2.0$ m. and $L_y = 1.0$ m

	$H/L_x = 0.1$				$H/L_x = 0.2$				
	$\eta = 0$	$\eta = 1$		$\eta = 3$		$\eta = 0$	$\eta = 1$		$\eta = 3$	
	Homog.	Graded	Homog.	Graded	Homog.	Homog.	Graded	Homog.	Graded	Homog.
1	71.706	56.373	56.385	53.832	53.835	46.540	42.877	42.883	41.149	41.158
2	132.873	255.767	255.778	245.005	245.030	66.290	115.273	115.286	108.695	108.734
3	461.391	414.363	414.381	358.085	358.096	129.285	160.573	160.587	160.546	160.578
4	536.205	643.820	643.821	634.201	634.212	209.350	217.103	217.110	202.055	202.137
5	771.798	746.508	746.496	716.112	716.115	236.953	241.962	241.964	229.723	229.790
6	855.896	1009.526	1009.527	999.648	999.647	273.515	286.176	286.181	269.468	269.547
7	911.411	1187.473	1187.466	1151.842	1151.817	300.456	334.597	334.583	322.338	322.544
8	1235.286	1257.901	1257.895	1277.630	1277.637	336.131	368.784	368.781	352.702	352.961
9	1329.886	1756.628	1756.619	1645.848	1645.847	386.992	456.753	456.751	429.349	430.047
10	1695.907	1770.750	1770.744	1864.465	1864.433	434.619	467.625	467.623	481.626	482.375

The change in natural frequencies does not show a clear pattern when going from $\eta = 1$ to $\eta = 3$. Most of the frequencies of the SSSS plate increased, while for the SFSF plate some increased and some decreased. The magnitude of the changes does not exhibit a clear pattern either. Some of them show the same change for the different aspect ratios, and the change is considerably different for others.

3.4. Magneto-Electro-Elastic Graded Composite Plates

As a final example, natural frequencies of composite plates consisting of a piezoelectric and a magnetostrictive phase are determined. These composites exhibit a magnetoelectric effect that is not present in the constituents. The coupled behavior between piezoelectric and magnetostrictive phases is represented by the magnetoelectric moduli d_{ij} that become non-zero as can be seen in Figure 1d. The plates considered in this example are made of the $BaTiO_3$-$CoFe_2O_4$ fibrous laminated composite material. The effective moduli are obtained based on the work published by Li and Dunn [3], in which a Mori-Tanaka mean field approach is used coupled with the magnetoelectroelastic Eshelby tensor to obtain explicit expressions for the effective magnetoelectroelastic and thermal moduli of two-phase composites. These composites consist of a magnetostrictive matrix with a dispersed fibrous piezoelectric phase. Here, we consider plates for which the volume fraction of the piezoelectric phase ($BaTiO_3$) continuously varies through the thickness

TABLE 9
Normalized natural frequencies of a rectangular Graphite/Epoxy plate with the orientation of the fibers continuously changing as a function of the thickness coordinate, and with $L_x = 2.0$ m., $L_y = 1.0$ m, two opposite edges simply supported and the remaining two free

	$H/L_x = 0.1$				$H/L_x = 0.2$				
	$\eta = 0$	$\eta = 1$		$\eta = 3$		$\eta = 0$	$\eta = 1$		$\eta = 3$	
	Homog	Graded	Homog.	Graded	Homog.	Homog.	Graded	Homog.	Graded	Homog.
1	2.667	2.710	2.711	2.960	2.961	1.917	1.911	1.911	2.092	2.093
2	5.513	5.939	5.939	6.201	6.201	2.757	3.097	3.097	3.142	3.142
3	5.513	10.369	10.369	9.038	9.039	2.757	5.102	5.102	4.457	4.458
4	6.871	10.793	10.795	10.245	10.245	5.046	6.995	6.996	7.056	7.056
5	11.027	10.933	10.937	12.453	12.457	5.513	7.458	7.461	7.612	7.614
6	12.771	17.741	17.741	17.403	17.397	7.362	8.857	8.861	8.388	8.390
7	14.055	18.099	18.105	18.274	18.279	7.774	9.101	9.102	9.389	9.390
8	15.077	18.635	18.640	18.588	18.588	8.270	11.450	11.453	11.014	11.017
9	15.743	23.068	23.071	20.696	20.695	8.270	12.157	12.159	11.454	11.457
10	16.540	25.784	25.786	24.595	24.599	8.672	12.410	12.411	11.597	11.597

TABLE 10
Normalized natural frequencies of a rectangular simply supported $BaTiO_3/CoFe_2O_4$ composite plate with the volume fraction of the constituents continuously changing as a function of the thickness coordinate, and with $L_x = 2.0$ m. and $L_y = 1.0$ m

	$H/L_x = 0.1$				$H/L_x = 0.2$			
	$\eta = 1$		$\eta = 3$		$\eta = 1$		$\eta = 3$	
	Graded	Homog.	Graded	Homog.	Graded	Homog.	Graded	Homog.
1	9.525	9.525	9.747	9.747	7.942	7.942	8.037	8.037
2	28.762	28.762	29.975	29.975	14.371	14.371	14.978	14.978
3	50.966	50.966	53.008	53.008	24.968	24.968	25.851	25.851
4	131.186	131.186	128.667	128.668	35.106	35.106	34.648	34.648
5	139.106	139.108	136.634	136.636	41.506	41.507	41.218	41.219
6	246.609	246.610	247.926	247.931	60.022	60.022	61.071	61.073
7	257.523	257.526	254.302	254.305	65.581	65.581	64.887	64.888
8	284.575	284.577	301.077	301.077	77.387	77.388	81.732	81.732
9	385.240	385.247	380.969	380.975	96.979	96.980	96.124	96.126
10	385.276	385.281	381.014	381.020	97.116	97.117	96.180	96.182

of the laminate according to Eq. (54) and repeated here for convenience

$$V_p(z) = \left(\frac{z}{H}\right)^{\eta} \tag{70}$$

$$V_m(z) = 1 - V_p(z) \tag{71}$$

The bottom surface of the plate is magnetostrictive ($CoFe_2O_4$) because the volume fraction of the piezoelectric phase (V_p) is zero, and the top surface is piezoelectric because the volume fraction of the magnetostrictive phase (V_m) is zero. Closed form expressions for the effective properties as published by Li and Dunn [3] are presented in Appendix B. In order to illustrate the through-thickness pre-integration for magneto-electro-elastic laminates, the first element of the elastic stiffness tensor is shown here and given by

$$C_{11}(z) = \frac{k_m k_p + V_p(z)k_p m_m + V_m(z)k_m m_m}{V_m(z)k_p + V_p(z)k_m + m_m} - \frac{m_m(k_m m_p + V_p(z)k_m m_p + V_m(z)k_m m_m + 2m_m m_p)}{V_m(z)k_m m_p + k_m m_m + V_p(z)k_m m_m + 2V_m(z)m_p m_m + 2V_p(z)m_m^2} \tag{72}$$

TABLE 11
Normalized natural frequencies of a rectangular $BaTiO_3/CoFe_2O_4$ composite plate with the volume fraction of the constituents continuously changing as a function of the thickness coordinate, and with $L_x = 2.0$ m., $L_y = 1.0$ m, two opposite edges simply supported and the remaining two free

	$H/L_x = 0.1$				$H/L_x = 0.2$			
	$\eta = 1$		$\eta = 3$		$\eta = 1$		$\eta = 3$	
	Graded	Homog.	Graded	Homog.	Graded	Homog.	Graded	Homog.
1	4.553	4.553	4.595	4.595	3.269	3.269	3.289	3.289
2	12.685	12.687	12.643	12.647	6.295	6.295	6.328	6.330
3	12.945	12.945	13.424	13.424	6.525	6.526	6.733	6.733
4	18.950	18.950	19.238	19.239	12.856	12.856	13.191	13.192
5	19.025	19.026	19.328	19.330	13.177	13.177	13.399	13.399
6	25.727	25.727	26.811	26.811	14.130	14.130	14.394	14.395
7	28.766	28.766	29.978	29.978	14.475	14.475	15.017	15.017
8	33.132	33.132	33.448	33.451	18.879	18.881	18.977	18.981
9	38.062	38.067	37.913	37.923	19.562	19.563	20.169	20.169
10	38.826	38.828	40.251	40.251	21.535	21.536	21.660	21.662

where the subscripts $_p$ and $_m$ indicate piezoelectric and magnetostrictive phases respectively, and k and m are the Hill moduli of the corresponding phases

$$k = \frac{C_{11} + C_{12}}{2} \tag{73}$$

$$m = \frac{C_{11} - C_{12}}{2} \tag{74}$$

Substitution of Eqs. (71) and (72) in Eq. (40) results in Eq. 75, which is the first component of the matrix $A_{\alpha\beta}$ representing the pre-integration with respect to the thickness coordinate. These integrals are evaluated numerically using 16 Gauss points before calculation of the natural frequencies. Normalized natural frequencies are shown in Tables 10 and 11, considering two different η values, and for the aspect ratios and support conditions mentioned before. Frequencies obtained using the homogenous layer approach are almost exactly the same as those calculated incorporating the gradation functions into the governing equations. The sense of change (increasing/decreasing) in frequencies of SSSS plates in going from $\eta = 1$ to $\eta = 3$ is the same for both aspect ratios, and the magnitude of the change is similar. However, for the SFSF plates having an aspect ratio $H/L_x = 0.10$, some of the frequencies decreased with the change in the variation of the volume fraction of the piezoelectric phase. On the other hand, all the frequencies increased with this change for the plates having an aspect ratio of 0.20. The magnitude of the changes were similar for both aspect ratios considered, with a maximum change of 4.2%.

$$A_{11}(z) = \int_{z_1}^{z_2} \left\{ \frac{k_m k_p + [(\frac{z}{H})^n] k_p m_m + [1 - (\frac{z}{H})^n] k_m m_m}{[1 - (\frac{z}{H})^n] k_p + [(\frac{z}{H})^n] k_m + m_m} \right.$$
$$\left. - \frac{m_m (k_m m_p + [(\frac{z}{H})^n] k_m m_p + [1 - (\frac{z}{H})^n] k_m m_m + 2 m_m m_p)}{[1 - (\frac{z}{H})^n] k_m m_p + k_m m_m + [(\frac{z}{H})^n] k_m m_m + 2[1 - (\frac{z}{H})^n] m_p m_m + 2[(\frac{z}{H})^n] m_m^2} \right\} \left(1 - \frac{z - z_1}{z_2 - z_1}\right)^2 dz \tag{75}$$

4. SUMMARY AND CONCLUSIONS

A discrete layer model has been developed and presented for the free-vibration analysis of magneto-electro-elastic graded plates. Two different approaches were developed: the first incorporates the function describing the through-thickness variation of the material properties into the governing equations, and the second considers the plates discretized into homogenous layers with properties determined by the average within the corresponding layer. The present model was validated with excellent agreement by comparing with the exact solution [19], the natural frequencies of a simply supported square metal-ceramic plate with the volume fraction of the constituents varying as functions of the thickness coordinate. The approaches presented here also were used to determine the natural frequencies of simply supported plates, and plates having two opposite edges simply supported and the other two free. Different materials and through-thickness gradation functions were considered: 1) isotropic metal-ceramic composite material for which the volume fraction of the phases varies through the thickness of the plate, 2) orthotropic material having an exponential variation of the elastic constants, 3) fiber reinforced composite material Graphite/Epoxy with a continuous variation of the fiber orientation, and 4) a magneto-electro-elastic composite material having a magnetostrictive matrix ($CoFe_2O_4$) reinforced with piezoelectric fibers ($BaTiO_3$) and considering a smooth variation of the volume fraction of the constituents as a function of the z-coordinate.

The main features and conclusions derived from the present work are listed below.

1. The discrete-layer model can be used to solve the free-vibration problem of magneto-electro-elastic graded plates with excellent accuracy when a sufficient number of layers and terms are employed in the approximations. Using 30 layers and one approximation term for the simply supported plates resulted in excellent agreement with exact solutions, while 30 layers and 7 terms for SFSF plate were sufficient to achieved convergence.
2. Any continuous function describing the gradient of the material properties can be successfully incorporated into the governing equations in the present approaches for the dynamic analysis of plates.
3. For the material parameters used, a uniform representation with homogeneous layers gives excellent accuracy, with the consequent reduction in effort and computational time. The maximum observed difference between approaches was only 0.3%. A similar homogenization technique have been successfully used by Shuvalovy and Soldatos [36] for the three-dimensional analysis of radially inhomogeneous tubes with an arbitrary cylindrical anisotropy, they showed that the exact formal solution may be approximated with any desired accuracy as far as the dimensionless thickness h of the layers is set anyhow small.
4. The effect of the gradation parameter η on the natural frequencies depends on the type of material and variation of material properties through the thickness of the plate. For the Al/ZrO_2 plate the frequencies increased when η was increased, while they decreased for the exponentially graded material, and for the graphite/epoxy and $BaTiO_3/CoFe_2O_4$ no obvious trend was observed.

5. REFERENCES

1. Benveniste, Y., "Magnetoelectric effect in fibrous composite with piezoelectric and piezomagnetic phases," *Physical Review B* **51**, 16424–16427 (1995).
2. Huang, J. H., and Kuo, W., "The analysis of piezoelectric/piezomagnetic composite materials containing ellipsoidal inclusions," *American Institute of Physics* **81**, 1378–1386 (1997).
3. Li, J. Y., and Dunn, M. L., "Micromechanics of magnetoelectroelastic composite materials; average fields and effective behavior," *Journal of Intelligent Material Systems and Structures* **9**, 404–416 (1998).
4. Aboudi, J., "Micromechanical analysis of fully coupled electro-magneto-thermo-elastic multiphase composites," *Smart Materials and Structures* **10**, 867–877 (2002).
5. Tan, P., and Tong, L., "Modeling for the electro-magneto-thermo-elastic properties of piezoelectric-magnetic fiber reinforced composites," Composites Part A: *Applied Science and Manufacturing* **33**, 631–645 (2002).
6. Pan, E., "Exact solution for simply supported and multilayered magneto-electro-elastic plates," *J. Appl. Mech.* **68**, 608–618 (2001).
7. Pan, E., and Heyliger, P. R., "Exact solutions for magnetoelectroelastic laminates in cylindrical bending," *Int. J. Solids Structures* **40**, 6859–6876, 2003.
8. Pan, E., and Heyliger, P. R., "Free vibration of simply-supported and multilayered magneto-electro-elastic plates," *Journal Sound Vibration* **252**, 429–442 (2002).
9. Heyliger, P. R., and Pan, E., "Static fields in magnetoelectroelastic lamintes," *AIAA Journal* **42**, 1435–1443 (2004).
10. Heyliger, P. R., Ramirez, F., and Pan, E., "Two-dimensional static fields in magnetoelectroelastic laminates," *Journal of Intelligent Material Systems and Structures* **15**, 689–709 (2004).
11. Jiang, A. M., and Ding, H. J., "Analytical solutions to magneto-electro-elastic beams," *Structural Engineering and Mechanics* **18**, 195–209 (2004).
12. Lage, R. G., Soares, C. M. M., Soares, C. A. M., and Reddy J. N., "Layer-wise partial mixed finite element analysis of magneto-electro-elastic plates," *Computer and Structures* **82**, 1293–1301 (2004).
13. Latheswary, S., Valsarajan, K. V., Rao, Y. V. K. S., "Dynamic response of moderately thick composite plates," *Journal of Sound and Vibration* **270**, 417–426 (2004).
14. Reddy, J. N., "Analysis of functionally graded plates," *Int. J. Numer. Meth. Engng.* **47**, 663–684 (2000).
15. Cheng, Z. Q., and Batra, R. C., "Deflection relationships between the homogeneous kirchhoff plate theory and different functionally graded plate theories," *Arch. Mech.* **52**, 143–58 (2000).
16. Cheng, Z. Q., and Batra, R. C., "Exact correspondence between eigenvalues of membranes and functionally graded simply supported polygonal plates," *J. Sound Vib.* **229**, 879–95 (2000).
17. Cheng, Z. Q., and Batra, R. C., "Three-dimensional thermoelastic deformations of a functionally graded elliptic plate," *Composites: Part B: Engineering* **31**, 97–106 (2000).
18. Vel S. S., and Batra, R. C., "Three-dimensional analysis of transient thermal stresses in functionally graded plates," *Int. J. Solids Struct.* **40**, 7181–7196 (2003).
19. Vel, S. S., and Batra, R. C., "Three-dimensional exact solution for the vibration of functionally graded rectangular plates," *J. Sound Vib.* **272**, 703–730 (2004).
20. Ferreira, A. J. M., Batra, R. C., Roque, C. M. C., Qian, L. F., Martins, P. A. L. S., "Static analysis of functionally graded plates using a third-order shear deformation theory ans a meshless method," *Composites Structures* **69**, 449–457 (2005).
21. Batra R. C., and Jin, J., "Natural frequencies of a functionally graded rectangular plate," *Journal of Sound and Vibration* **282**, 509–516 (2005).
22. Qian, L. F., Batra, R. C., and Chen, L. M., "Static and dynamic deformations of thick functionally graded elastic plates by using higher-order shear and normal deformable plate theory and meshless Petrov-Galerkin Method," Composites Part B: *Engineering* **35**, 685–697 (2004).
23. Pan, E., "Exact solution for functionally graded anisotropic elastic composite laminates," *Journal of Composite Materials* **37**, 1903–1919 (2003).
24. Ramirez, F., Heyliger, P. R., and Pan, E., "Static analysis of functionally graded elastic anisotropic plates using a discrete layer approach," Composites B—*Engineering* **37**, 10–20 (2006).
25. Yang, J., Kitipornchai, S., and Liew, K. M., "Non-linear analysis of the thermo-electro-mechanical behaviour of shear deformable fgm plates with piezoelectric actuators," *International Journal for Numerical Methods in Engineering* **59**, 1605–1632 (2004).
26. Woo, J., and Meguid, S. A., "Nonlinear analysis of functionally graded plates and shallow shells," *International Journal of Solids and Structures* **38**, 7409–7421 (2001).
27. Liew, K. M., Sivashanker, S., He, X. Q., and Ng, T. Y., "The modelling and design of smart structures using functionally graded materials and piezoelectrical sensor/actuator patches," *Smart Materials and Structures* **12**, 647–655 (2003).
28. Buchanan, G. R., "Layered *versus multiphase magneto-electro-elastic composites*," Composites Part B—*Engineering* **35**, 413–420 (2004).
29. Chen, W. Q., Ding, H. J., and Hangzhou, P. R., "On free vibration of a functionally graded piezoelectric rectangular plate," *Acta Mechanica* **153**, 207–216 (2002).
30. Chen, W. Q., Lee, K. Y., and Ding, H. J., "On free vibration of non-homogeneous transversely isotropic magneto-electro-elastic plates," *Journal of Sound and Vibration* **279**, 237–251 (2005).
31. Harshe, G., Dougherty, J. P., and Newnham, R. E., "Theoretical modeling of multilayer magnetoelectric composites," *Int. J. Appl. Electromag* **4**, 145–159 (1993).
32. Reddy, J. N., *Energy and Variational Methods in Applied Mechanics*, John Wiley and Sons, New York (1984).
33. Reddy, J. N., *Mechanics of Laminated Composite Plates: Theory and Analysis* 2nd Ed., CRC Press, Boca Raton, FL (1997).
34. Reddy, J. N., "A generalization of displacement-based laminate theories," *Communications in Applied Numerical Methods* **3**, 173–181 (1987).
35. Vel S. S., (Private communication).
36. Shuvalovy, A. L., and Soldatos, K. P., "On the successive approximation method for three-dimensional analysis of radially inhomogeneous tubes with an arbitrary cylindrical anisotropy," *Journal of Sound and Vibration* **259**, 233–239 (2003).

APPENDIX A

Tensor Transformation Equations

$$C_{11} = C^o_{11}\cos^4\theta + C^o_{22}\sin^4\theta + 2\sin^2\theta\cos^2\theta\left(C^o_{12} + 2C^o_{66}\right) \tag{76}$$

$$C_{22} = C^o_{11}\sin^4\theta + C^o_{22}\cos^4\theta + 2\sin^2\theta\cos^2\theta\left(C^o_{12} + 2C^o_{66}\right) \tag{77}$$

$$C_{33} = C^o_{33} \tag{78}$$

$$C_{44} = C^o_{44}\cos^2(\theta) + C^o_{55}\sin^2(\theta) \tag{79}$$

$$C_{55} = C^o_{44}\sin^2(\theta) + C^o_{55}\cos^2(\theta) \tag{80}$$

$$C_{66} = \left(C^o_{11} - 2C^o_{12} + C^o_{22}\right)\cos^2\theta\sin^2\theta + C^o_{66}(\cos^2\theta - \sin^2\theta)^2 \tag{81}$$

$$C_{12} = \left(C^o_{11} - 4C^o_{66} + C^o_{22}\right)\cos^2\theta\sin^2\theta + C^o_{12}(\cos^4\theta + \sin^4\theta) \tag{82}$$

$$C_{13} = C^o_{13}\cos^2\theta + C^o_{23}\sin^2\theta \tag{83}$$

$$C_{23} = C_{13}^o \sin^2\theta + C_{23}^o \cos^2\theta \quad (84)$$

$$C_{45} = \left(C_{55}^o - C_{44}^o\right)\cos\theta\sin\theta \quad (85)$$

$$C_{16} = \left[\left(C_{11}^o - 2C_{66}^o - C_{12}^o\right)\cos^2\theta + \left(C_{11}^o + 2C_{66}^o - C_{22}^o\right)\sin^2\theta\right]\cos\theta\sin\theta \quad (86)$$

$$C_{26} = \left[\left(C_{11}^o - 2C_{66}^o - C_{12}^o\right)\sin^2\theta + \left(C_{11}^o + 2C_{66}^o - C_{22}^o\right)\cos^2\theta\right]\cos\theta\sin\theta \quad (87)$$

$$C_{36} = \left(C_{13}^o - C_{23}^o\right)\cos\theta\sin\theta \quad (88)$$

APPENDIX B

Magneto-Electro-Elastic Effective Moduli [3]

Elastic Moduli:

$$C_{11}(z) = C_{22}(z) = k(z) + m(z) \quad (89)$$

$$C_{33}(z) = C_{33m} + V_p(z) \times \left[C_{33p} - C_{33m} - \frac{V_m(z)(C_{13m} - C_{13p})^2}{V_m(z)k_p + V_p(z)k_m + m_m}\right] \quad (90)$$

$$C_{13}(z) = C_{23}(z) = C_{13m} + \frac{V_p(z)(C_{13p} - C_{13m})(k_m + m_m)}{V_m(z)k_p + V_p(z)k_m + m_m} \quad (91)$$

$$C_{12}(z) = k(z) - m(z) \quad (92)$$

$$C_{44}(z) = C_{55}(z) = C_{44m} + j\left[(e_{15p} - e_{15m})(fe - gh) + (C_{44p} - C_{44m}) \times (ih - fd) + (q_{15p} - q_{15m})(gd - ie)\right] C_{66}(z) = m(z) \quad (93)$$

$$C_{66}(z) = m(z) \quad (94)$$

$$k(z) = \frac{k_m k_p + V_p(z)k_p m_m + V_m(z)k_m m_m}{V_m(z)k_p + V_p(z)k_m + m_m} \quad (95)$$

$$m(z) = \frac{m_m(k_m m_p + V_p(z)k_m m_p + V_m(z)k_m m_m + 2m_m m_p)}{V_m(z)k_m m_p + k_m m_m + V_p(z)k_m m_m + 2V_m(z)m_p m_m + 2V_p(z)m_m^2} \quad (96)$$

Piezoelectric Coefficents:

$$e_{31}(z) = e_{32}(z) = e_{31m} + \frac{V_p(z)(e_{31p} - e_{31m})(k_m + m_m)}{V_m(z)k_p + V_p(z)k_m + m_m} \quad (97)$$

$$e_{33}(z) = e_{33m} + V_p(z) \times \left[e_{33p} - e_{33m} + \frac{V_m(z)(C_{13m} - C_{13p})(e_{31p} - e_{31m})}{V_m(z)k_p + V_p(z)k_m + m_m}\right] \quad (98)$$

$$e_{15}(z) = e_{24}(z) = e_{15m} + j[(e_{15p} - e_{15m})(ga - fc) + (C_{44p} - C_{44m})(fb - ia) + (q_{15p} - q_{15m})(ic - gb)] \quad (99)$$

Piezomagnetic Coefficients:

$$q_{31}(z) = q_{32}(z) = q_{31m} + \frac{V_p(z)(q_{31p} - q_{31m})(k_m + m_m)}{V_m(z)k_p + V_p(z)k_m + m_m} \quad (100)$$

$$q_{33}(z) = q_{33m} + V_p(z) \times \left[q_{33p} - q_{33m} + \frac{V_m(z)(C_{13m} - C_{13p})(q_{31p} - q_{31m})}{V_m(z)k_p + V_p(z)k_m + m_m}\right] \quad (101)$$

$$q_{15}(z) = q_{24}(z) = q_{15m} + j\left[(e_{15p} - e_{15m})(ch - ae) + (C_{44p} - C_{44m})(ad - bh) + (q_{15p} - q_{15m})(be - cd)\right] \quad (102)$$

Dielectric Permittivity Moduli:

$$\epsilon_{11}(z) = \epsilon_{22}(z) = \epsilon_{11m} + j[(\epsilon_{11p} - \epsilon_{11m})(ga - fc) + (e_{15p} - e_{15m})(ia - fb) + (\mu_{11p} - \mu_{11m})(ic - gb)] \quad (103)$$

$$\epsilon_{33}(z) = \epsilon_{33m} + V_p(z) \times \left[\epsilon_{33p} - \epsilon_{33m} - \frac{V_m(z)(e_{31p} - e_{31m})^2}{V_m(z)k_p + V_p(z)k_m + m_m}\right] \quad (104)$$

Magnetic Permittivity Moduli:

$$\mu_{11}(z) = \mu_{22}(z) = \mu_{11m} + j[(d_{11p} - d_{11m})(ch - ae) + (q_{15p} - q_{15m})(bh - ad) + (\mu_{11p} - \mu_{11m})(be - cd)] \quad (105)$$

$$\mu_{33}(z) = \mu_{33m} + V_p(z) \times \left[\mu_{33p} - \mu_{33m} - \frac{V_m(z)(\mu_{31p} - \mu_{31m})^2}{V_m(z)k_p + V_p(z)k_m + m_m}\right] \quad (106)$$

Magnetoelectric Coefficients;

$$d_{11}(z) = d_{22}(z) = d_{11m} + j[(\epsilon_{11p} - \epsilon_{11m})(ch - ae) + (e_{15p} - e_{15m})(bh - ad) + (d_{11p} - d_{11m})(be - cd)] \quad (107)$$

$$d_{33}(z) = d_{33m} + V_p(z) \times \left[d_{33p} - d_{33m} - \frac{V_m(z)(e_{31p} - e_{31m})(q_{31m} - q_{31p})}{V_m(z)k_p + V_p(z)k_m + m_m}\right] \quad (108)$$

Constants:

$$j(z) = 2V_p(z)\frac{[C_{44m}\epsilon_{11m}\mu_{11m} + e_{15m}^2\mu_{11m} + \epsilon_{11m}q_{15m}^2 - 2d_{11m}e_{15m}q_{15m} - d_{11m}^2C_{44m}]}{(ic-gb)h + (fb-ia)e + (ga-fc)d} \tag{109}$$

$$a(z) = [(q_{15p}-q_{15m})(\epsilon_{11m}\mu_{11m} - d_{11m}^2) - (d_{11p}-d_{11m})(e_{15m}\mu_{11m} - d_{11m}q_{15m}) - (\mu_{11p}-\mu_{11m})(q_{15m}\epsilon_{11m} - d_{11m}e_{15m})]V_m(z) \tag{110}$$

$$b(z) = [(e_{15p}-e_{15m})(\epsilon_{11m}\mu_{11m} - d_{11m}^2) - (d_{11p}-d_{11m})(q_{15m}\epsilon_{11m} - d_{11m}e_{15m}) - (\epsilon_{11p}-\epsilon_{11m})(e_{15m}\mu_{11m} - d_{11m}q_{15m})]V_m(z) \tag{111}$$

$$c(z) = [(C_{44p}-C_{44m})(\epsilon_{11m}\mu_{11m} - d_{11m}^2) + (e_{15p}-e_{15m})(e_{15m}\mu_{11m} - d_{11m}q_{15m}) + (q_{15p}-q_{15m})(q_{15m}\epsilon_{11m} - d_{11m}e_{15m})] \times V_m(z) + \frac{j}{2}[(ic-gb)h + (fb-ia)e + (ga-fc)d] \tag{112}$$

$$d(z) = [-(d_{11p}-d_{11m})(d_{11m}C_{44m} + e_{15m}q_{15m}) + (e_{15p}-e_{15m})(e_{15m}\mu_{11m} - d_{11m}q_{15m}) + (\epsilon_{11p}-\epsilon_{11m})(q_{15m}^2 + C_{44m}\mu_{11m})] \times V_m(z) + \frac{j}{2}[(ic-gb)h + (fb-ia)e + (ga-fc)d] \tag{113}$$

$$e(z) = [(q_{15p}-q_{15m})(d_{11m}C_{44m} + e_{15m}q_{15m}) + (C_{44p}-C_{44m})(e_{15m}\mu_{11m} - d_{11m}q_{15m}) - (e_{15p}-e_{15m})(q_{15m}^2 + C_{44m}\mu_{11m})]V_m(z) \tag{114}$$

$$f(z) = [-(d_{11p}-d_{11m})(d_{11m}C_{44m} + e_{15m}q_{15m}) + (q_{15p}-q_{15m})(q_{15m}\epsilon_{11m} - d_{11m}e_{15m}) + (\mu_{11p}-\mu_{11m})(e_{15m}^2 + C_{44m}\epsilon_{11m})] \times V_m(z) + \frac{j}{2}[(ic-gb)h + (fb-ia)e + (ga-fc)d] \tag{115}$$

$$g(z) = [(e_{15p}-e_{15m})(d_{11m}C_{44m} + e_{15m}q_{15m}) + (C_{44p}-C_{44m})(q_{15m}\epsilon_{11m} - d_{11m}e_{15m}) - (q_{15p}-q_{15m})(e_{15m}^2 + C_{44m}\epsilon_{11m})]V_m(z) \tag{116}$$

$$h(z) = [(q_{15p}-q_{15m})(\mu_{11m}e_{15m} + d_{11m}q_{15m}) - (\mu_{11p}-\mu_{11m})(C_{44m}d_{11m} - e_{15m}q_{15m}) + (d_{11p}-d_{11m})(q_{15m}^2 + C_{44m}\mu_{11m})]V_m(z) \tag{117}$$

$$i(z) = [(e_{15p}-e_{15m})(\epsilon_{11m}q_{15m} - d_{11m}e_{15m}) - (\epsilon_{11p}-\epsilon_{11m})(C_{44m}d_{11m} - e_{15m}q_{15m}) + (d_{11p}-d_{11m})(e_{15m}^2 + C_{44m}\epsilon_{11m})]V_m(z) \tag{118}$$